Materials Advances

ROYAL SOCIETY OF CHEMISTRY

PAPER

View Article Online
View Journal | View Issue

Cite this: *Mater. Adv.*, 2025, 6, 6174

4D printed polymethacrylate lattices capable of dimensional switching and payload release *via* photoresponsive actuation of azobenzene units

James MacKay,[a] Lewis R. Hart,[a] Alarqam Z. Tareq,[ab] Simeng Wang,[c] Valeria Gonzalez Abrego,[c] Ian Maskery,[c] Derek Irvine,[c] Ricky D. Wildman[c] and Wayne Hayes *[a]

Received 24th June 2025,
Accepted 1st August 2025

DOI: 10.1039/d5ma00670h

rsc.li/materials-advances

In this report, we demonstrate the synthesis of photoresponsive polymeric hydrogel lattices using stereolithographic 3D printing to afford objects that can change shape when irradiated with UV-vis light. Methacrylate-based monomers featuring azobenzene units were used as the photo-actuator components. Co-polymerisation of these monomers with 2-hydroxyethyl methacrylate produced well-defined hydrogel lattices. Photo-actuation of the hydrogels led to contraction of the 3D printed lattices up to 23% by volume. The ability of such photoresponsive hydrogel lattices to exhibit payload release has been studied using methylene blue as a drug mimic. Upon irradiation, the hydrogel lattice was squeezed like a sponge through photo-induced actuation in pulses, resulting in the controlled release of the pro-drug over 24 hours.

Introduction

Additive manufacturing, or 3D printing[1,2] has emerged as a manufacturing tool for producing bespoke, tailored objects in a multitude of materials.[3,4] This rapidly developing technology was initially regarded as a prototyping tool, but more recently has been used successfully in fields such as drug delivery,[5–8] regenerative and medicine,[9,10] magnetics,[11,12] and sensors,[13–15] exploiting the capability to produce highly complex 3D structures.[16] Additive manufacturing techniques are generally classified into seven categories (see ISO/ASTM 52900), but the technologies most commonly adopted include vat polymerisation,[17] extrusion printing,[18] ink jet printing,[19] and powder bed fusion.[20,21] Each of these methodologies relies on different technologies to produce 3D constructs and requires different physical properties of materials in order to achieve good printability.

A more recent direction has been a focus on how the benefits of design freedom can be integrated with those offered by freedom of function (*e.g.* surface reactivity, dynamic shape changes, modification of colour, gradient properties) that arise from the constituent materials used in their construction. Advanced polymer design now works hand in hand with the control of additive manufacturing to realise highly functional devices.[22,23] For example, the use of responsive polymeric materials[24–26] has allowed access to so-called '4D printing'[27–29] in which parts undergo primarily shape change in response to an appropriate stimulus after being manufactured. Introducing a reversible shape change or adjustment of the physical properties of the 3D printed component in response to an external stimulus enables the production of ever more complex structures which can perform a work function.[30]

Structural elements whose dimensional characteristics can be addressed remotely without physical or chemical intervention are extremely attractive. One such moiety of particular interest is the photoactive azobenzene motif.[31] The reversible photo-induced trans-cis isomerisation[32] of the azobenzene motif has been utilised successfully in rotaxanes[33] by Murakami *et al.* to afford a molecular switch. Furthermore, Ji and co-workers have reported[34] the development of a bilayer actuator containing pendant azobenzene units. Upon exposure to light, the bilayer shape exhibited reversible deflection with photo generated stresses ranging from 1.03 to 1.70 MPa. Stoddart and co-workers[35] have reported photoresponsive hydrogel featuring azobenzene units whose photoisomerisation plays an important role in the sol–gel phase transition. Photoresponsive surface liquid crystal-based coatings with dynamic protrusions were successfully developed by Broer and co-workers *via* incorporation of azobenzene units into cross-linked polymer networks.[36–38] Building on these reports, liquid crystal

[a] *Department of Chemistry, University of Reading, Whiteknights, Reading, RG6 6AD, UK. E-mail: w.c.hayes@reading.ac.uk*
[b] *Department of Chemistry, Faculty of Science, University of Zakho, Duhok 42001, Iraq*
[c] *Faculty of Engineering, The University of Nottingham, University Park, Nottingham, NG7 2RD, UK*

elastomers with biomimetic properties were developed by Feringa, Broer and co-workers which were used in inks for 3D printing to generate adaptive soft materials that were responsive to light.[39,40] The photoinduced isomerisation of integrated azobenzene units within the elastomer initiates a change of the order of the liquid crystal molecular units in the network. In addition, Ware and co-workers described the use of an azobenzene liquid crystal supramolecular elastomer to generate a Braille-like actuator.[41] The printed Braille sheets featured 6 dots which could be raised for up to 24 hours post irradiation with UV light; heating the image to 65 °C enabled regeneration of the original flat structure.

In this study, we sought to demonstrate how we could combine the design freedoms offered by additive manufacturing with bespoke photoresponsive polymer lattices to afford controlled release of a payload. The potential for such dynamic 3D printed devices lies in the development of new drug delivery systems or light activated pumps. We report the synthesis of two methacrylate monomers featuring azobenzene substituents and their copolymerisation with a biocompatible 2-hydroxyethyl methacrylate (HEMA) monomer *via* stereolithography to generate complex 3D lattices with well-defined channels. These structures formed gels in water before being exposed to UV light leading to successful actuation of the lattices[42] whereby well-defined shape change was realised with a contraction of the 3D printed polymers up to 23% by volume.

Results and discussion

To create a photo-actuated 3D printed device, which could be addressed by light to alter its dimensions in a precise and spatially controlled fashion, a complex 3D polymeric lattice was envisaged. Specifically, the lattice would be formulated from a photoresponsive moiety which could be co-polymerised with a hydrogelating monomer to yield a flexible polymer matric which can impart motion. This soft matrix could therefore act as a host for an application specific payload, such as a therapeutic or drug, which, upon irradiation with a specific wavelength of light could undergo a significant reduction in dimensions and expel or deliver the cargo (Scheme 1).

In order to create a soft polymer matrix which was able to deflect or deform when actuated by appropriate stimulation, HEMA was chosen as the hydrogelator component of the 3D printed lattice. 3D printing of HEMA by stereolithographic techniques has been established. Furthermore, HEMA displays excellent biocompatibility, as demonstrated by its use in medical devices such as contact lenses. These attractive properties would allow for a 3D printed biomedical device to be realised which could be used in drug delivery settings. To facilitate the desired dimensional changes in the proposed lattice structure, a network was designed which could respond to a specific stimulus, such as UV light, with a significant reduction in its volume whilst still retaining its structural integrity. To this end, a monomer based on methacrylate functionalities decorated with azobenzene motifs was designed to impart motion on the resulting molecular machine. The azobenzene moiety is known to undergo a *trans*-to-*cis* isomerisation upon irradiation with UV light, with the *trans*-isomer exhibiting a greater end-to-end distance (*ca.* 9 Å) than the *cis* conformation (*ca.* 5 Å), representing a dimensional change of *ca.* 44%.[43–45] Furthermore, the *trans*-isomer is the most energetically stable form of azobenzene, thus allowing for a shape/volume reduction to be realised upon stimulation on demand. It was therefore proposed that a lattice structure comprising of an appropriate loading of azobenzene units as either cross-linkers or pendant functional groups should lead to a stimuli responsive system.

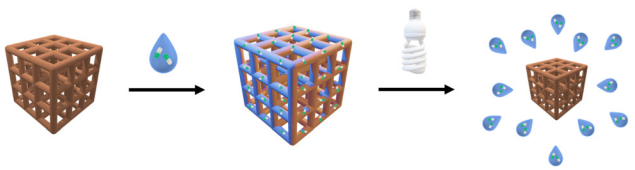

Scheme 1 Schematic representation of a regular hydrogelating lattice structure capable of uptake of a payload and release of that cargo upon photoactivation.

To facilitate the required molecular motion, a photoresponsive monomer with a single polymerisable terminal **1** in addition to a cross-linkable molecular actuator **2** were designed, both featuring azobenzene motifs (Scheme 2). More specifically, monomer **1** was synthesised by the esterification of the commercially available 4-(phenylazo)benzoic acid with HEMA[46] to yield the desired molecular actuator. Similarly, monomer **2** was prepared by first synthesising azobenzene-4,4-dicarboxylic acid by the reduction of 4-nitrobenzoic acid with glucose, resulting in an orange precipitate which was brought forward without further purification, and esterifying with HEMA. The successful synthesis of the monomer **1** and **2** was confirmed by FTIR, ^{1}H NMR, and ^{13}C NMR spectroscopic analysis. The full synthetic procedures and the characterisation data for monomers **1** and **2** can be found in the SI (see Fig. S1–S17). The ^{1}H NMR spectra of the monomer **1** and **2** reveals three resonances at *ca.* 6.46 ppm, *ca.* 5.60 ppm, and *ca.* 1.96 ppm, which correspond to the protons of alkene functional groups in the structure of HEMA. ^{13}C NMR spectroscopy corroborated the formation of the ester linkages in the monomer **1** and **2** with resonances observed at *ca.* 166 ppm. In addition, two absorbance bands were observed at 1631–1638 cm^{-1} and 1707–1711 cm^{-1} in the FTIR spectra were attributed to the incorporation of the methacrylate alkane and carbonyl stretches of the ester and groups, respectively.

With the desired azobenzene monomers in hand, initial investigations were focused on exploring the photoisomerisation of the novel monomers in solution. To achieve this, the optical properties of the novel monomers were assessed by UV-visible spectroscopy (see Fig. S18) which revealed two distinct absorbances (Fig. 1). The first absorbance (**1**; λ_{max} = 329 nm, ε = 80 200 dm^3 mol^{-1} cm^{-1} and **2**; λ_{max} = 330 nm, ε = 82 400 dm^3 mol^{-1} cm^{-1}) corresponded to a $\pi^* \leftarrow \pi$ transition, whilst the second, lower intensity absorbance centred at 450 nm (**1**; ε = 2200 dm^3 mol^{-1} cm^{-1} and **2**; ε = 5840 dm^3 mol^{-1} cm^{-1}) corresponded to a $\pi^* \leftarrow$ n transition.[47] Solution phase photoisomerization of the azobenzene derived

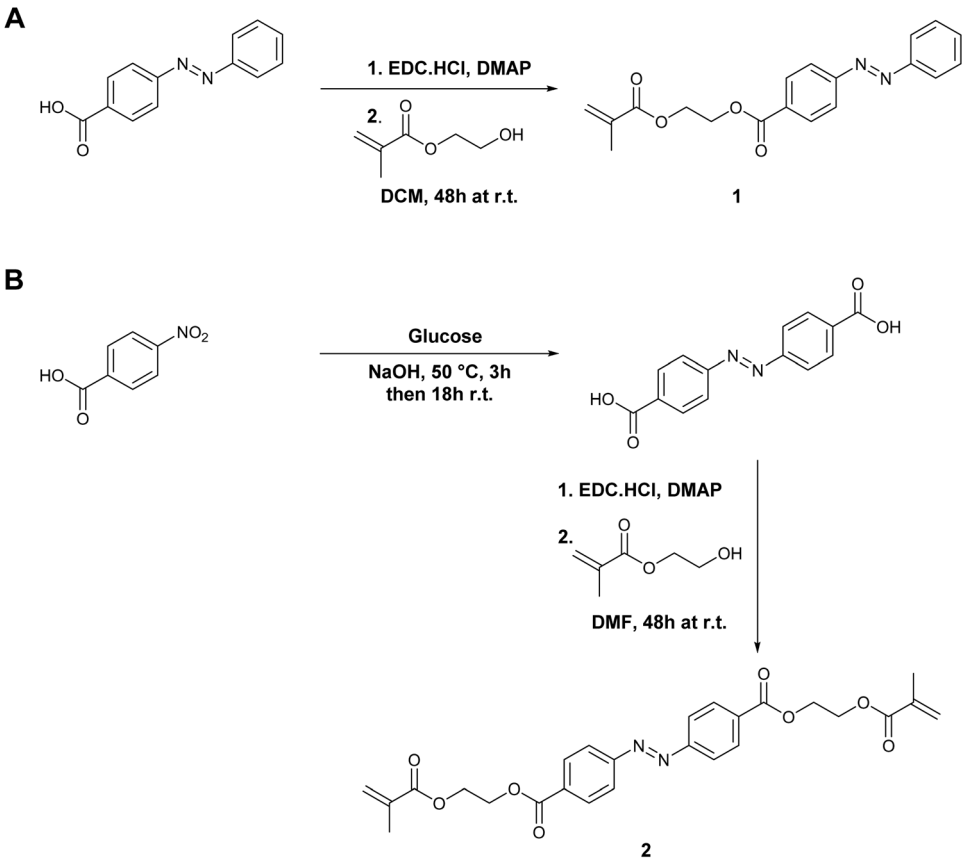

Scheme 2 Synthesis of the photoresponsive monomers **1** and **2** from their azobenzene carboxylic acid precursors.

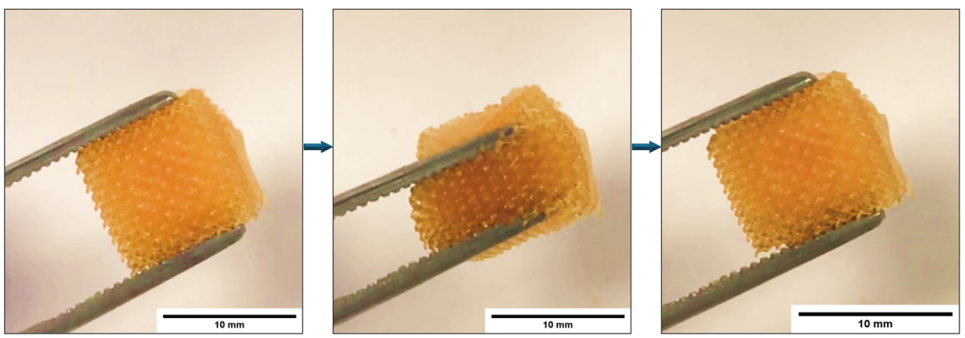

Fig. 1 Deformation of the 3D printed polymer diamond lattice afforded from formulation **F8**.

monomers **1** and **2** was subsequently induced by application of UV light (320 nm, 25 W) with the wavelength output matching the absorbance bands of the photoresponsive monomers. Upon absorption, the $\pi^* \leftarrow \pi$ transition band at *ca.* 330 nm exhibited a decrease in intensity while conversely the absorbance associated with the $\pi^* \leftarrow$ n transition (λ = 450 nm) increased in intensity. Indeed, observed change in absorbance intensities was indicative of *trans*-to-*cis* isomerisation, through the increased adsorption of the $\pi^* \leftarrow$ n absorbance which is known to become more intense upon the formation of the *cis* isomer *via* the rotational pathway.[47] By plotting the decrease in the intensity of peak observed at *ca.* 330 nm with respect to time (Fig. S19), the rate of isomerisation was assessed and followed an exponential decay, reaching 90% conversion of the theoretical minimum after 2 minutes. Irradiation of the sample for a further 8 minutes revealed no further decrease in the absorption at λ_{max}. The reverse *cis*-to-*trans* isomerisation was also accessed by application of visible light which restored the absorbance at *ca.* 330 nm to its maximum after *ca.* 25 minutes (Fig. S20). These rates are similar to those reported for structurally related compounds.[48] Furthermore, the thermal *cis*-to-*trans* isomerisation was also investigated in the dark from which no significant change in absorbance was observed over a 60 minute period, agreeing with reported literature with half-lives of related compounds at room temperature.[49]

Preliminary additive manufacturing studies were carried out using an Asiga Pico 39 Plus (18 mW cm^{-1}, λ_{max} = 385 nm), with novel HEMA derived formulations, in addition to an Asiga Flash UV lightbox to post-cure for 6 minutes. Subsequent printing of lattice structures were carried out using an AnyCubic mono 4K LCD printer. Phenylbis(2,4,6-trimethylbenzoyl) phosphine oxide (BAPO, a Norrish type 1 photoinitiator) was employed as the photoinitiator in the generation of the lattice structures using concentrations between 1 mol% and 5 mol% and irradiation times between 20 and 60 seconds. The optimum photoinitiator concentration was found to be 1.5 mol% with the formulations used and irradiation for 50 seconds per layer gave rise to the most promising results with well-defined structures formed. With appropriate conditions in hand, 3D printing studies were carried out using eight formulations with increasing concentrations of monofunctional **1** and difunctional **2** monomers (see Table 1). Initial efforts were focused on the stereolithographic printing of difunctional monomer **2** with HEMA to afford solid lattices. Lattices were constructed from formulations **F1–F4**, but the resolution of these structures thus produced was deemed not acceptable for the desired application. However, promisingly these lattice structures did swell and soften when immersed in water for 24 hours. In an attempt to improve the resolution and volume changes of the resulting hydrogelator, the monofunctional monomer **1** was introduced to the formulation matrix (formulations **F5–F8**). It was proposed that the trans-to-cis photo-isomerisation of monofunctional azobenzene monomer **1** may require less energy than the difunctional analogue **2** owing since the isomerisable unit is not covalently bound at both ends and may improve the UV induced actuation of the polymer network. Incorporation of monofunctional monomer **1** into the printing formulation **F5–F8** was successfully achieved, as demonstrated by the elevation in the glass transition temperature (T_g) of the material from *ca.* 70 °C to *ca.* 110 °C. The increase in T_g values could be attributed to the hydrogen bonding between HEMA chains[50,51] as well as the effect of the pendant nature of the azobenzene as side chain moieties within the polymer network.[52] Monomer **2** behaved as a crosslinker during photopolymerisation and thus movement of aromatic units were restricted by covalent bonds. Interestingly, the resolution of the printed lattices also improved relative to prints with only monomer **2** and HEMA. The printing of lattice structures using **F7** and **F8** were also attempted on a AnyCubic mono 4K LCD printer (12 W, 405 nm). This printer offered a larger printing area than the Asagi Pico 39 Plus printer (105.6 cm^2 compared to 15.6 cm^2) while offering an improved in resolution of 35 μm relative to 39 μm. A longer exposure time (60–90 seconds) was required to delivery high resolution lattice, However, up to 60 pieces of 1 cm^3 were printed successfully in a single attempt thanks to the large printable area.

Table 1 Composition and thermal properties of the formulations 3D printed

Formulation	Monomer **1** (mol%)	Monomer **2** (mol%)	HEMA (mol%)	BAPO 10 (mol%)	T_g (°C)
F1	0.00	0.25	98.25	1.50	80
F2	0.00	0.50	98.00	1.50	—
F3	0.00	0.75	97.75	1.50	77
F4	0.00	1.00	97.50	1.50	76
F5	0.125	0.13	98.25	1.50	111
F6	0.25	0.25	98.00	1.50	110
F7	0.5	0.25	97.75	1.50	105
F8	0.25	0.5	97.75	1.50	110

To examine the hydration of the 3D printed polymeric hydrogels, diamond (5 × 5 × 5 mm) and gyroid lattice cubes (10 × 10 × 10 mm) were printed from formulations **F1–F8** and swollen in water at room temperature for 24 hours. The soft hydrogelating polymer lattices were compliant enough to be deformed by gentle squeezing with tweezers (see Fig. 1, Video S1 and Fig. S21) and returned to its original shape once the force was removed.

In order to manufacture a robust, yet flexible, structure from the hydrogelating monomers which could undergo a controlled change in shape and volume, a number of designs and printed lattices were screened, see Fig. S22–S26. Whilst solid cubic shapes were first explored using HEMA as the monomer, these did not provide enough freedom of motion when hydrated to allow for shape-changes and were therefore were excluded. To promote deformation in the structure, a series of strut- and surface-based lattice structures were selected for further investigations. Lattices are now commonly used in additive manufacturing on account of their innately modifiable properties. Their strength and stiffness, for example, can be tailored through selection of unit cell geometry, volume fraction and constituent material. This makes lattices desirable for a range of applications, including regenerative medicine, where matching the mechanical properties of a printed part to that of healthy organic tissue is important.[53,54] For the application described here, the open connected structures of lattices provide a further exploitable property – they allow high throughput of light to the internal structure. The high surface-to-volume ratio of lattices is also beneficial in that it promotes gelation, while the high percentage of void space thus enables mobility of polymer struts under light actuation.

Compression testing was employed to further assess the effect of hydration on the properties of the 3D printed lattices. The printed diamond lattice cubes were submerged in water at room temperature for increasing periods of time then subjected to compression to a force of 100 N. As the hydration time of the diamond lattice cube was increased, the deformation under load also increased (Fig. 2). The time taken for a diamond lattice cube to fully hydrate was between 3 and 4 days, with no further significant change in the compression after 4 days of hydration at ambient room temperature. On increasing the temperature of the water to 50 °C (below the T_g of the polymers), the time taken to hydrate the diamond lattice cubes was reduced from approximately 4 days to 30 hours (Fig. S27).

To assess the properties of the swollen hydrogel, the hydrated 3D printed polymer networks **F1–F8** were subject to rheological testing after being fully hydrated. In all hydrogels of formulations **F1–F8** the storage modulus G' was greater than the loss modulus G'' indicating that the elastic component

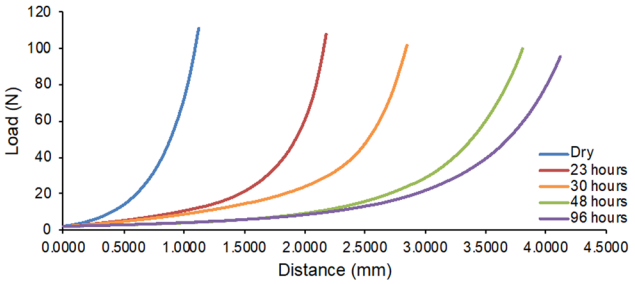

Fig. 2 Compression testing of a 3D printed diamond lattice cube **F8**. Each series indicates a different submersion time in water at room temperature.

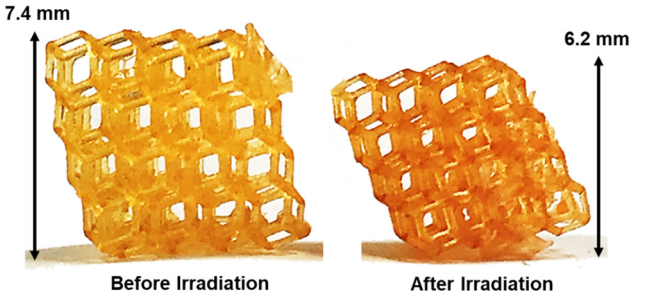

Fig. 3 Octahedral structure of 3D printed formulation **F7** before and after UV irradiation.

Table 2 Rheological property evaluation of 3D printed formulations under a constant strain of 0.1%, and values of G' and G'' have been applied as a function of applied frequency in the whole regime from 0.1 to 10 Hz

Formulation No.	Log G' (Pa) (10^4)	Log G'' (Pa) (10^4)
F1	5.41	1.80
F2	5.92	1.97
F3	5.47	2.43
F4	3.62	1.15
F5	4.51	1.57
F6	8.61	3.30
F7	12.28	4.49
F8	5.76	1.67

Table 3 Shrinkage results for different formulations and lattice structures

Formulation No.	Lattice	Shrinkage (%vol/vol)
F1	Octahedral	8.85
F3	Octahedral	2.64
F5	Octahedral	7.72
F6	Octahedral	21.1
F7	Octahedral	22.9
F8	Octahedral	14.8
F7	Gyroid	5.2

dominates in these materials (Table 2). Additionally, G' and G'' were independent of one another at a constant temperature and behaved in a linear fashion with respect to shear rate, demonstrating classical gel like behaviour. Plotting the concentration of monomer **2** against G' and G'' revealed that hydrogel **F2** and **F8** with 0.5 mol% monomer **2** exhibited the highest elastic nature, with the material's elastic contribution decreasing at a greater rate than its viscous contribution as the concentration of monomer **2** is increased (Fig. S28). This result is in good agreement with the results from the compression testing experiment, with a weaker polymer hydrogel formed when increased concentrations of difunctional monomer **2** were used.

In order for the 3D printed structure to be used as a molecular actuator, the polymers must be able to deform, reduce in volume and expel its payload. To assess the photo-actuation of the polymeric hydrogel, the shape and volume change of the 3D printed polymer samples was analysed. The 3D printed diamond, gyroid and octahedral lattices structures were tested for their ability to contract by first measuring the external dimensions of the lattice before hydrating them in water (see Fig. S29). The hydrated objects where then subjected to high-intensity UV light (320 nm, 240 W) allowing for the photoisomerisation of azobenzene moieties. As the size and volume of the object changed, this was frozen by the evaporation of the water, decreasing the mobility of the polymer chains and preventing the *cis*-to-*trans* isomerisation in visible light once complete, allowing for accurate measurements to be made (see Fig. 3 and Fig. S30).

When reviewing the results from shrinkage experiments, it was apparent that octahedral lattice allowed for a greater degree of volume change when compared to the diamond lattice cubes (Table 3). The octahedral lattice permits increased light penetration to the centre of the structure, allowing for greater actuation when the polymer was irradiated with UV light. When considering the shrinkage results for the different formulations, it was realised that incorporation of the monofunctional monomer, **1**, increased the amount of shrinkage possible in the system. This may have been a result of the hydrated polymeric network being softened by monofunctional monomer **1** which does not cross-link the network, reducing the energy barrier to isomerise and deform. Formulations **F6** and **F7** resulted in the highest levels of actuation (see Table 3). Both formulations contained the same amount of difunctional monomer **2** (0.25 mol%) but different levels of monofunctional monomer **1** (0.25 and 0.5 mol%, respectively). Within this preliminary study, the effect of actuation of monofunctional **1** on the hydrated polymer network reached a limit with formulation **F6**. The equivalent concentration of difunctional monomer **2** in both formulations resulted in similar volume changes.

To investigate the ability of the polymers to reform their original volume through the reverse *cis*-to-*trans* photoisomerisation, the 3D printed polymer hydrogels were exposed to ambient light conditions for 3 days. While many of the polymer hydrogels exhibited a high level of recovery of their original volume, other lattices showed almost no change. Structures with the octahedral architecture were best able to regain their shape and volume *via* the reverse photoisomerisation as this structure appears to accommodate such dimensional adjustments when compared to the diamond lattice. Interestingly, formulations containing the monofunctional monomer **1** returned more readily to their original shape, demonstrating the importance of the balance between cross-linking and molecular isomerisation.

To further optimise the shape and volume change in the photoresponsive polymer hydrogel, a more extensive screening in lattice design was undertaken. Lattice structures based on

the gyroid minimal surface were designed using in-house AM design software.[55] Each lattice had dimensions of (10 × 10 × 10) mm, with cell numbers along each direction of between 3 and 7. The lattices possessed volume fractions (*i.e.*, the ratio of solid volume to total volume) between 0.05 and 0.15. The gyroid lattice was chosen for this study as its manufacturability with a range of AM processes has been widely demonstrated[56,57] and it has greater specific surface area than many conventional, strut-based designs. From the screening study, a lattice with a cell wall size of 10 mm and 3 unit cells provided the best printed structures (Fig. 4A and B).

In order to review the effect of the photo-induced isomerisation of the hydrogel on the release of a model payload, methylene blue was incorporated into the resin formulation. As methylene blue has a low absorbance at 385 nm, the dye was not expected to interfere with the printing by absorbing the UV radiation. As methylene blue has a high extinction coefficient (ε = 87 000 M^{-1} cm^{-1}) and absorbs in a region where the other materials in the formulation had a minimal absorbance (λ_{max} = 660 nm), making it an ideal analyte to track the release of the formulation's payload. The payload was incorporated into formulation **F7**, which showed the highest amount of UV induced contraction, at a concentration of 0.6 mol%. The resin was printed using print parameters described above which resulted in the dye being successfully dispersed within the polymer network as exemplified by the deep blue colour of the structure. Interestingly, the lattice structures showed an improved definition over previous prints without the dye (Fig. 4C). Galagan *et al.* have reported[58] that ethylene blue is able to react with radicals to form a semi reduced species during a polymerisation. The semi-reduced methylene blue radical could then react with another radical species, leading to termination of both radicals and thus the polymerisation. The ability of methylene blue to react with radicals may have allowed for an increased number of termination events during the propagation of the polymer in the 3D printer, resulting in an increased resolution in the 3D printed structures with no change in the required exposure time between printed layers.

To explore the effect of photoisomerisation on release of the payload, several copies of the lattice structure containing methylene blue (0.6 mol%) were printed. The lattices were first washed thoroughly with acetone and THF, dried under ambient conditions before being immersed in acetone for 24 hours to remove any residual methylene blue dye from the surface of the printed structures. The lattices were then transferred into a vial containing 5 mL of acetone. One of the samples was placed in a sealed box and exposed to UV radiation (302 nm, 8 W) whilst another identically prepared lattice was exposed to ambient conditions with natural light (as a control). Aliquots of the solvent (20 μL) were taken from both samples at 1 hour intervals across a period of 8 hours. The two lattice/acetone samples were held under the same conditions overnight and two further samples were taken at the 24th and 25th hour. The aliquots extracted from the solution phase were diluted in 4 mL of distilled water. 100 μL of the diluted extracts were transferred into a 24-well plate and further diluted with 900 μL distilled water. The level of methylene blue extracted was quantified using a plate reader by measuring the absorbance at 495 nm. These tests were repeated three times, and a distinct trend was found (see Fig. 5). In the first 24 hours, the printed lattices subjected to UV radiation revealed a significant increase in absorbance in stark contrast to the control sample under

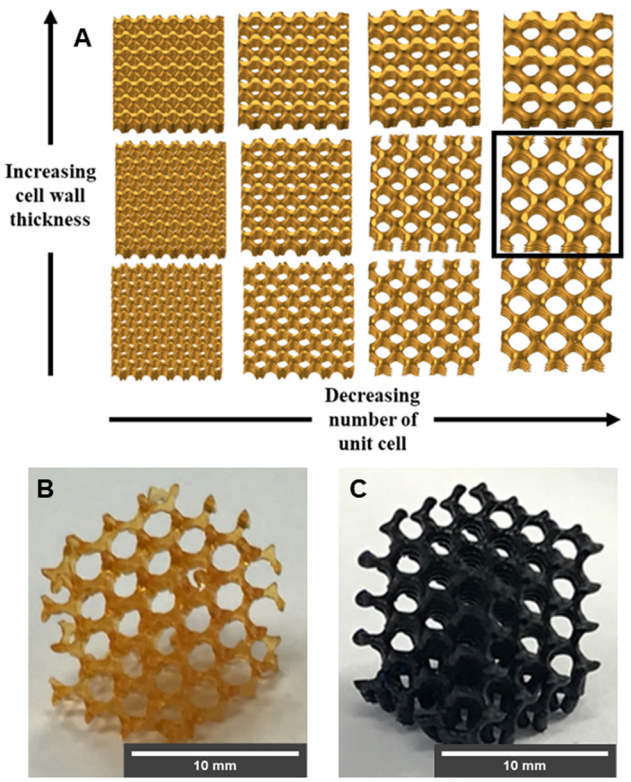

Fig. 4 (A) Lattice designs with increasing cell wall thickness and decreasing number of unit cells, (**B**) the highlighted design was found to have the best printed resolution (insert), (**C**) 3D Printed lattice of formulation **F7** containing 0.6 mol% of methylene blue.

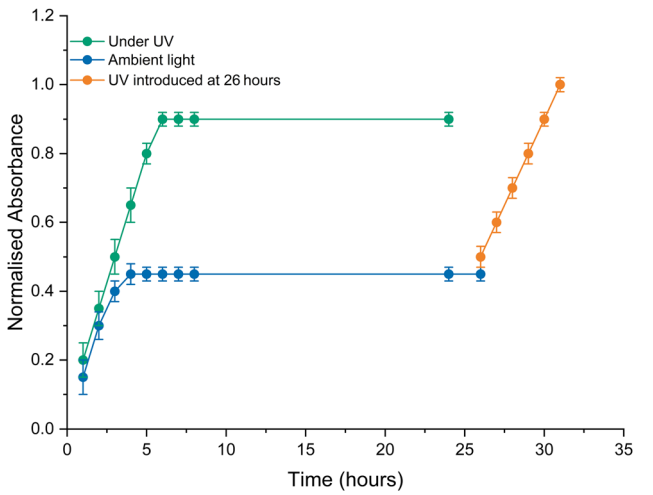

Fig. 5 Absorbance values from the UV-vis spectra of the release of methylene blue from lattices printed from formulation **F7** containing methylene blue dye.

ambient light. For the lattice held under ambient conditions, the release of methylene blue plateaued after three hours, whereas the lattice exposed to UV radiation continued to release dye at a consistent rate up to six hours. In addition, the absorbance of the sample exposed to UV was approximately twice as high than the sample under ambient light. This data shows that exposing the printed lattices doped with methylene blue to UV radiation was effective in increasing both the release rate, and the quantity of the dye released. It is proposed that the lattices doped with methylene blue held under ambient light releases dye predominantly by diffusion, and that the process becomes less efficient after the dye near the lattice surface has been extracted. In contrast, the lattice exposed to UV radiation could release more dye and at a faster rate as the dyes were expelled by the contraction of the lattice, in addition to the diffusion process.

To validate this, the control samples under ambient light were exposed to UV radiation after 25 hours. After three hours, the concentration of methylene blue solution of this lattice remained approximately constant. However, the concentration of methylene blue increased in the acetone supernatant after the introduction of the UV radiation, attaining approximately the same release level as the lattice directly exposed to UV radiation after 6 hours. This 'stepped' release profile proved that the UV radiation induced contraction of 3D printed lattices featuring the azo monomers **1** and **2** was effective in increasing the efficiency of substrate release.

Conclusions

In this paper, we have demonstrated the synthesis of polymeric hydrogel lattices *via* stereolithographic 3D printing which are photoresponsive and change shape when irradiated with UV-vis light. Methacrylate monomers featuring azobenzenes were used as photo-actuator units. The monomers were then copolymerised using a stereolithography 3D printer with a known biocompatible monomer, namely 2-hydroxyethyl methacrylate, to produce hydrogel lattices. Photo-actuation of the hydrogel was readily accomplished, resulting in contraction of the 3D printed lattice up to 23% by volume. The photoresponsive hydrogel lattice has the potential to be used in applications such customisable drug delivery devices as demonstrated by the photo-activated release of a drug mimic, methylene blue. Upon irradiation, the hydrogel lattice was squeezed like a sponge in several pulses through photo-induced actuation, resulting in the controlled release of the pro-drug over a 24 hour period.

Experimental

Materials

Reagents and solvents were purchased from Sigma Aldrich, TCI, and Fisher Scientific and were used without further purification. The synthesis and characterisation data of the compounds and polymers described in this paper are reported in the SI file.

Characterisation

^{1}H NMR (400 MHz) and ^{13}C NMR (100 MHz) spectra were obtained on a Bruker Nanobay 400 or a Bruker DPX 400 spectrometer using 2M deuterated sodium hydroxide as solvent. Infrared (IR) spectroscopic analysis was carried out using a PerkinElmer 100 FTIR instrument with diamond-ATR sampling accessory and samples either as solids or oils. Mass spectra were recorded from on an Orbitrap XL using ESI as an ionisation technique. Ultraviolet-visible spectra were measured with a Varian Cary 300 spectrophotometer or an Agilent Cary 3500 UV-vis Multicell Peltier UV spectrophotometer with heating attachment, using 1 cm^2 quartz cuvettes, in the wavelength range 350–800 nm. Subsequent dye release test samples were measured on a Tecan Infinite M Plex plate reader. Differential scanning calorimetry (DSC) was carried out using a TA Instruments Q2000 calorimeter. Samples for DSC were heated to 110 °C to remove residual solvent, cooled to −90 °C, and then re-scanned from −90 to 250 °C. Rheological profiles of the polymers were assessed by a Malvern Kinexus Lab+, with an 8 mm plate geometry and 8 mm pedestal running rSpace 1.76 software. Printed discs of 8 mm diameter, 1 mm thickness were analysed over a frequency range from 10 Hz to 0.1 Hz at 37 °C. The storage (G') and loss modulus (G'') were recorded over the frequency sweep. An AML Instruments™ Single Column Tensometer (Thümler Z3-X1200) accompanied by THSSD-2019 RC10 software was used for compression testing. Compression testing consisted of crushing 5 mm^3 cubes at a rate of 10 mm min^{-1} up to a maximum load of 100 N. UV exposure to assess the photo-contraction properties of the polymers was provided by a Rayonet RPR-200. The photochemical reactor features a sample platform surrounded by sixteen 14 W 9″ UV lamps outputting 320 nm light. Exposure times varied from 1 to 72 hours as required. Parts were measured before hydration with water and immediately following UV exposure. The dye release test employed a Thermo Scientific 3UV Lamp (302 nm, 8 W) as the UV source.

3D printing

The initial 3D printing was performed on an Asiga Pico 39 Plus, using Asiga Composer software to edit and upload STL files. All prints were performed with a layer height of 50 μm. A 1 mm baseplate was used to adhere the parts to the build platform, using twice the exposure time as the rest of the print. 5 mm support structures to allow for removal of the parts from the build platform. Printed parts were then washed with 2-propanol (prints using Plaswhite) or THF (prints using HEMA 3) to remove any unreacted monomer and low molecular weight oligomer gels from the structures. Post-curing was performed in an Asiga Flash UV lightbox for 6 minutes, turning the parts halfway through to ensure an even cure. The printing was subsequently performed in an AnyCubic mono 4K LCD printer (405 nm) for larger scale printing. The STL files were sliced at 50 μm per layer with ChituBox slicer software (V1.9.5). A base layer of 250 μm was used to increase adhesion of the prints to the build plate. The printed parts were rinsed with acetone and THF to remove the excess resin. The washed parts were dried in ambient condition and post-cured for 10 minutes using AnyCubic Wash & Cure 2.0 (405 nm).

Release and uptake studies

To formulation **F7** was added methylene blue (0.6 mol%). The formulation was printed on AnyCubic Mono 4K 3D printer following the printing (90 s exposure time) and cleaning procedure described. Before the extraction, the dark blue printed structures were further cleaned by washing with THF (3 × 10 mL) and acetone (10 mL) and dried. The dry prints were weighed before immersing in clean acetone for 24 hours. Two swollen structures were rinsed with acetone and dried with paper towel. The dried swollen lattices were placed in a vial containing clean acetone (5 mL). One of which was placed in a sealed box and exposed to 302 nm, 8 W UV light while the other structures were left in visible lighting conditions as control. An aliquot (20 μL) the acetone of both samples was taken at regular intervals and diluted in 4 mL of distilled water. 100 μL of the resultant solution was placed in a 24-well plate before the analysis and further diluted with 900 μL of distilled water. The UV-visible spectroscopy analysis was performed on a Tecan Infinite M Plex plate reader. The experiment was repeated 3 times. The plots obtained were normalised with respect to the mass of the dry print. The relative quantity of the methylene blue released from each set was estimated by the absorbance at 659 nm.

Conflicts of interest

There are no conflicts of interest to declare.

Data availability

The data supporting this article have been included as part of the SI.

Synthetic protocols for the monomers, characterisation data for these compounds, 3D lattice designs and images of the 3D printed lattices. See DOI: **https://doi.org/10.1039/d5ma00670h**.

Acknowledgements

The authors from the University of Reading and the University of Nottingham would like to acknowledge funding from EPSRC (EP/N024818/1) in support of a postdoctoral fellowships for LRH in addition to Ian Maskery and Simeng Wang (EP/W017032/1), and HECD Iraq for providing a PhD studentship for AZT. The authors would also like to thank the University of Reading for access to analytical instrumentation within the Chemical Analysis Facility. The authors acknowledge the practical assistance from Professor Ian Hamley at the University of Reading at the outset of the studies.

References

1 S. C. Ligon, R. Liska, J. Stampfl, M. Gurr and R. Mülhaupt, *Chem. Rev.*, 2017, **117**, 10212–10290.
2 T. O. Machado, C. J. Stubbs, V. Chiaradia, M. A. Alraddadi, A. Brandolese, J. C. Worch and A. P. Dove, *Nature*, 2024, **629**, 1069–1074.
3 D. E. Fagnani, J. L. Tami, G. Copley, M. N. Clemons, Y. D. Y. L. Getzler and A. J. McNeil, *ACS Macro Lett.*, 2021, **10**, 41–53.
4 A. Bagheri and J. Jin, *ACS Appl. Polym. Mater.*, 2019, **1**, 593–611.
5 L. Ruiz-Cantu, G. F. Trindade, V. Taresco, Z. Zhou, Y. He, L. Burroughs, E. A. Clark, F. R. A. J. Rose, C. Tuck, R. Hague, C. J. Roberts, M. Alexander, D. J. Irvine and R. D. Wildman, *ACS Appl. Mater. Interfaces*, 2021, **13**, 38969–38978.
6 Y. He, R. Foralosso, G. F. Trindade, A. Ilchev, L. Ruiz-Cantu, E. A. Clark, S. Khaled, R. J. M. Hague, C. J. Tuck, F. R. A. J. Rose, G. Mantovani, D. J. Irvine, C. J. Roberts and R. D. Wildman, *Adv. Ther.*, 2020, **3**, 1900187.
7 I. Louzao, B. Koch, V. Taresco, L. Ruiz-Cantu, D. J. Irvine, C. J. Roberts, C. Tuck, C. Alexander, R. Hague, R. Wildman and M. R. Alexander, *ACS Appl. Mater. Interfaces*, 2022, **14**(6), 8654.
8 P. Das, S. Ganguly, P. K. Marvi, M. Sherazee, S. R. Ahmed, X. Tang, S. Srinivasan and A. R. Rajabzadeh, *Adv. Funct. Mater.*, 2024, **34**, 2314520.
9 L. Ouyang, J. P. K. Armstrong, Y. Lin, J. P. Wojciechowski, C. Lee-Reeves, D. Hachim, K. Zhou, J. A. Burdick and M. M. Stevens, *Sci. Adv.*, 2020, **6**, eabc5529.
10 Y. S. Zhang, A. Dolatshahi-Pirouz and G. Orive, *Science*, 2024, **385**, 604–606.
11 M. Garibaldi, I. Ashcroft, M. Simonelli and R. Hague, *Acta Mater.*, 2016, **110**, 207–216.
12 A. Milleret, V. Laitinen, K. Ullakko, N. Fenineche and M. M. Attallah, *Addit. Manuf.*, 2022, **60**, 103231.
13 M. R. Khosravani and T. Reinicke, *Sens. Actuators, A*, 2020, **305**, 111916.
14 J. Lee and H. So, *Microsyst. Nanoeng.*, 2023, **9**, 44.
15 Y. Jiang, M. N. Islam, R. He, X. Huang, P.-F. Cao, R. C. Advincula, N. Dahotre, P. Dong, H. F. Wu and W. Choi, *Adv. Mater. Technol.*, 2023, **8**, 2200492.
16 M. Baumers, C. Tuck, R. Wildman, I. Ashcroft and R. Hague, *J. Ind. Ecol.*, 2017, **21**, S157–S167.
17 S. Zakeri, M. Vippola and E. Levänen, *Addit. Manuf.*, 2020, **35**, 101177.
18 J. Yu, Y. Xu, S. Li, G. V. Seifert and M. L. Becker, *Biomacromolecules*, 2017, **18**, 4171–4183.
19 Y. Gu, X. Chen, J.-H. Lee, D. A. Monteiro, H. Wang and W. Y. Lee, *Acta Biomater.*, 2012, **8**, 424–431.
20 N. T. Aboulkhair, M. Simonelli, L. Parry, I. Ashcroft, C. Tuck and R. Hague, *Prog. Mater. Sci.*, 2019, **106**, 100578.
21 R. D. Goodridge, C. J. Tuck and R. J. M. Hague, *Prog. Mater. Sci.*, 2012, **57**, 229–267.
22 L. Li, Q. Lin, M. Tang, A. J. E. Duncan and C. Ke, *Chem. – Eur. J.*, 2019, **25**, 10768–10781.
23 L. R. Hart, A. B. R. Touré, R. Owen, N. R. E. Putri, R. J. M. Hague, M. R. Alexander, F. R. A. J. Rose, Z. Zhou, D. J. Irvine, L. Ruiz-Cantu, L. Turyanska, Y. He, W. Hayes and R. D. Wildman, *Mater. Today Commun.*, 2025, **45**, 112206.
24 A. D. O'Donnell, S. Salimi, L. R. Hart, T. S. Babra, B. W. Greenland and W. Hayes, *React. Funct. Polym.*, 2022, **172**, 105209.

25 A. Subash and B. Kandasubramanian, *Eur. Polym. J.*, 2020, **134**, 109771.
26 J. Chen, C. Virrueta, S. Zhang, C. Mao and J. Wang, *Mater. Today*, 2024, **77**, 66–91.
27 H. Wei, Q. Zhang, Y. Yao, L. Liu, Y. Liu and J. Leng, *ACS Appl. Mater. Interfaces*, 2017, **9**, 876–883.
28 X. Xia, J. Meng, J. Qin, G. Yang, P. Xuan, Y. Huang, W. Fan, Y. Gu, F. Lai and T. Liu, *ACS Appl. Polym. Mater.*, 2024, **6**, 3170–3178.
29 P. Rastogi and B. Kandasubramanian, *Chem. Eng. J.*, 2019, **366**, 264–304.
30 B. Du, Y. He, M. Shen, Z. Hu, W. Fu, J. Zou, R. Huang and T. Yu, *J. Polym. Sci.*, 2024, **62**, 4809–4834.
31 E. R. Talaty and J. C. Fargo, *Chem. Commun.*, 1967, 65–66, DOI: 10.1039/C19670000065.
32 A. A. Beharry and G. A. Woolley, *Chem. Soc. Rev.*, 2011, **40**, 4422–4437.
33 H. Murakami, A. Kawabuchi, K. Kotoo, M. Kunitake and N. Nakashima, *J. Am. Chem. Soc.*, 1997, **119**, 7605–7606.
34 D. E. Hagaman, S. Leist, J. Zhou and H.-F. Ji, *ACS Appl. Mater. Interfaces*, 2018, **10**, 27308–27315.
35 Y.-L. Zhao and J. F. Stoddart, *Langmuir*, 2009, **25**, 8442–8446.
36 A. H. Gelebart, D. Jan Mulder, M. Varga, A. Konya, G. Vantomme, E. W. Meijer, R. L. B. Selinger and D. J. Broer, *Nature*, 2017, **546**, 632–636.
37 D. Liu, C. W. M. Bastiaansen, J. M. J. den Toonder and D. J. Broer, *Macromolecules*, 2012, **45**, 8005–8012.
38 D. Liu, C. W. M. Bastiaansen, J. M. J. den Toonder and D. J. Broer, *Angew. Chem., Int. Ed.*, 2012, **51**, 892–896.
39 G. Long, Y. Deng, W. Zhao, G. Zhou, D. J. Broer, B. L. Feringa and J. Chen, *J. Am. Chem. Soc.*, 2024, **146**, 13894–13902.
40 S. J. Wezenberg, C. M. Croisetu, M. C. A. Stuart and B. L. Feringa, *Chem. Sci.*, 2016, **7**, 4341–4346.
41 X. Lu, C. P. Ambulo, S. Wang, L. K. Rivera-Tarazona, H. Kim, K. Searles and T. H. Ware, *Angew. Chem., Int. Ed.*, 2021, **60**, 5536–5543.
42 M. Baroncini, S. d'Agostino, G. Bergamini, P. Ceroni, A. Comotti, P. Sozzani, I. Bassanetti, F. Grepioni, T. M. Hernandez, S. Silvi, M. Venturi and A. Credi, *Nat. Chem.*, 2015, **7**, 634–640.
43 E. Wagner-Wysiecka, N. Łukasik, J. F. Biernat and E. Luboch, *J. Inclusion Phenom. Macrocyclic Chem.*, 2018, **90**, 189–257.
44 M. Zhu and H. Zhou, *Org. Biomol. Chem.*, 2018, **16**, 8434–8445.
45 C. Renner, U. Kusebauch, M. Löweneck, A. G. Milbradt and L. Moroder, *J. Pept. Res.*, 2005, **65**, 4–14.
46 Y.-Y. Xiao, X.-L. Gong, Y. Kang, Z.-C. Jiang, S. Zhang and B.-J. Li, *Chem. Commun.*, 2016, **52**, 10609–10612.
47 A. A. Beharry, O. Sadovski and G. A. Woolley, *J. Am. Chem. Soc.*, 2011, **133**, 19684–19687.
48 L. H. Urner, B. N. S. Thota, O. Nachtigall, S. Warnke, G. von Helden, R. Haag and K. Pagel, *Chem. Commun.*, 2015, **51**, 8801–8804.
49 H. M. D. Bandara and S. C. Burdette, *Chem. Soc. Rev.*, 2012, **41**, 1809–1825.
50 L. Qie and M. A. Dubé, *Int. J. Adhes. Adhes.*, 2010, **30**, 654–664.
51 M. Fernández-Garcia, M. F. Torrado, G. Martinez, M. Sánchez-Chaves and E. L. Madruga, *Polymer*, 2000, **41**, 8001–8008.
52 R. Xie, A. R. Weisen, Y. Lee, M. A. Aplan, A. M. Fenton, A. E. Masucci, F. Kempe, M. Sommer, C. W. Pester, R. H. Colby and E. D. Gomez, *Nat. Commun.*, 2020, **11**, 893.
53 A. Krivitsky, N. Paunović, K. Klein, F. B. Coulter, S. Schleich, A. A. Karol, A. Bauer, V. Krivitsky, V. Lohmann, P. C. Carril, Y. Bao, B. von Rechenberg, C. Halin, A. R. Studart, D. Franzen and J.-C. Leroux, *J. Controlled Release*, 2025, **377**, 553–562.
54 Y. Yuts, R. McCabe, M. Krell, M. Bohley and J.-C. Leroux, *Int. J. Pharm.*, 2025, **669**, 125051.
55 I. Maskery, L. A. Parry, D. Padrão, R. J. M. Hague and I. A. Ashcroft, *Addit. Manuf.*, 2022, **49**, 102510.
56 I. Maskery, L. Sturm, A. O. Aremu, A. Panesar, C. B. Williams, C. J. Tuck, R. D. Wildman, I. A. Ashcroft and R. J. M. Hague, *Polymer*, 2018, **152**, 62–71.
57 I. Maskery, N. T. Aboulkhair, A. O. Aremu, C. J. Tuck, I. A. Ashcroft, R. D. Wildman and R. J. M. Hague, *Mater. Sci. Eng., A*, 2016, **670**, 264–274.
58 Y. Galagan and W.-F. Su, *J. Photochem. Photobiol., A*, 2008, **195**, 378–383.